LONGITUDINAL SPACE-CHARGE EFFECTS IN A RETARDING FIELD ENERGY ANALYZER

Y. Zou[*], Y. Cui, I. Haber, M. Reiser and P.G. O'Shea, Institute for Research in Electronics and Applied Physics, University of Maryland, College Park, MD 20742, USA

Abstract

Experimental and theoretical work has been carried out to study the longitudinal space-charge effects in a retarding field energy analyzer. A one-dimensional model for both a mono-energetic beam and a thermal beam has been developed for this purpose. The study shows that, if the current density inside the device were higher than a critical value, the longitudinal space-charge effects would distort the measured energy spectrum. The measured mean energy will be shifted toward the low-energy side and the resulting spectrum will have a tail at the high-energy side. The measured FWHM and rms energy spread may also be affected.

INTRODUCTION

In order to characterize the energy spread in UMER [1], a retarding field energy analyzer has been developed and tested. The design and testing results of the device have been reported elsewhere [2, 3]. During the experiment, it was found that, when the current density in the analyzer is higher than a certain value, the measured energy spectrum is shifted towards the low-energy side compared to the one measured with low injected current. Fig. 1 depicts such a case, where Curve I is for a low-current case and Curve II is for a high-current case. At the same time, the energy spectrum measured with high current density has a tail at high-energy side. This is believed to be due to the longitudinal space-charge force in the device. The mean energy shift due to the space-charge effect was observed before in studies of the energy spread in a beam from an ion source, for example see Refs. [4, 5]. Ref. [6] gave an approximate analytical solution to explain the space-charge effect in the ion source, the result of which is similar to the Langmuir-Child equation. In this paper, we will, via analytical analysis and simulations, present new results for the longitudinal space-charge effect in this kind of devices.
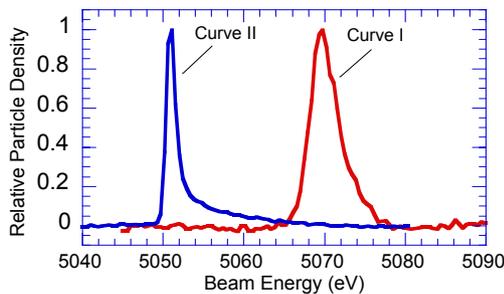
Fig. 1. Experimental result of energy spectrum. Injected current for Curve I is 0.2 mA, for Curve II is 2.2 mA.

[*]Email: yunzou@glue.umd.edu

FIELD SOLUTIONS FOR A MONO-ENERGETIC BEAM

The potential distribution in such a system is described by a one-dimensional Poisson equation:

$$\frac{d^2V}{dz^2} = -\frac{\rho}{\varepsilon_0} = -\frac{J}{\varepsilon_0 \sqrt{\frac{2q(V+V_0)}{m}}} = CJ(V+V_0)^{-1/2} \tag{1}$$

Here, C is a constant defined as $C = -1/\left(\varepsilon_0 (2q/m)^{1/2}\right)$. J is the current density and ε_0 is free space permittivity. V is the potential relative to the lab ground and V_0 is the voltage equivalent of the injected beam energy. The general solutions to this differential equation can be solved under three different regimes. The first regime is that V_r is a small negative voltage relative to the lab ground, in which case the potential distribution has a minimum with magnitude smaller than V_0. In the second regime, V_r is moderately large such that the potential decreases monotonically from ground to V_r. The third regime is that V_r is large enough such that the magnitude of the potential minimum is equal to V_0. This is equivalent to the virtual cathode formation in the electron gun and the beam particles start to be reflected back by this potential bump [7].

The solution to the first regime is given by

$$-\frac{3c_1}{4}(z-X_m) = \tag{2}$$
$$\left((V(z)+V_0)^{1/2}+c_2\right)^{3/2} - 3c_2\left((V(z)+V_0)^{1/2}+c_2\right)^{1/2}$$

for $0<z<X_m$, and

$$\frac{3c_1}{4}(z-X_m) = \tag{3}$$
$$\left((V(z)+V_0)^{1/2}+c_2\right)^{3/2} - 3c_2\left((V(z)+V_0)^{1/2}+c_2\right)^{1/2}$$

for $X_m<z<d_r$.

Here $c_1 = \sqrt{4CJ_0}$, where J_0 is the injected current density. X_m is the location of the potential minimum; c_2 is an unknown constant. d_r is the total length of the device. X_m and c_2 are determined by the boundary condition:

$$\begin{cases} V(z)=0, & z=0 \\ V(z)=V_r, & z=d_r \end{cases} \tag{4}$$

In the second regime, the potential decreases monotonically from zero to V_r and the solution is given by:

$$-\frac{3c_1}{4}z =$$

$$\left[\left((V(z)+V_0)^{1/2}+c_2\right)^{3/2}-\left((V(0)+V_0)^{1/2}+c_2\right)^{3/2}\right] \quad , (5)$$

$$-3c_2\left[\left((V(z)+V_0)^{1/2}+c_2\right)^{1/2}-\left((V(0)+V_0)^{1/2}+c_2\right)^{1/2}\right]$$

where c_1 is the same constant as in the first regime and c_2 is an unknown constant determined by the boundary conditions.

In the third regime, the virtual cathode forms. The potential distribution is given by

$$V(z)+V_0 =$$
$$\left(\frac{3}{4}\right)^{4/3}(4CJ_1)^{2/3}(X_m-z)^{4/3} \qquad 0<z<X_m \qquad (6)$$

and

$$V(z)+V_0 =$$
$$\left(\frac{3}{4}\right)^{4/3}(4CJ_2)^{2/3}(z-X_m)^{4/3} \qquad X_m<z<d_r \qquad (7)$$

Here J_1 and J_2 are given by

$$J_1 = (2-p)J_0 \quad 0<z<X_m$$
$$J_2 = pJ_0 \qquad X_m<z<d_r \qquad (8)$$

In Eqs.(6) and (7), the unknown constants are X_m and p, which are determined by the boundary conditions. The formation of the virtual cathode only happens when the beam current density inside the energy analyzer is larger than a limiting current. The magnitude of the limiting current is given by

$$J_{\lim} = \left(\frac{3}{4}\right)^2 \frac{1}{4Cd_r^2}V_0^{3/2}, \qquad (9)$$

which has the same format as Child's law. For convenience, we introduce a concept of normalized current density $\lambda=J_0/J_{lim}$, the ratio of the injected beam current density to the limiting current density J_{lim}. Fig. 2 shows the energy analyzer response to a monoenergetic beam with beam energy of 5 keV and normalized input current density of 0.8 and 1.4 respectively. For λ=0.8, the spectrum reveals the real beam spectrum, while for higher current, λ=1.4, the energy spectrum is shifted towards the low-energy side due to the space charge.
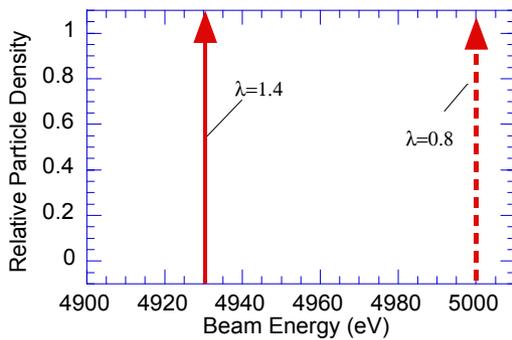
Fig. 2. Spectrum at different current densities.

FIELD SOLUTIONS FOR A THERMAL BEAM

At the entrance of the energy analyzer, the thermal beam has the following initial phase-space distribution

$$f_i(z=0,v_i) = f_0 \exp\left(-\alpha^2(v_i-v_0)^2\right), \qquad (10)$$

where $\alpha = \sqrt{m/(2k_BT_i)}$ is related to the beam energy spread. v_0 is the mean beam velocity. f_0 is the normalization factor. After particles enter the energy analyzer, the distribution becomes:

$$f_z(v_z) = f_0 \exp\left(-\alpha^2\left(\sqrt{v_z^2-2\eta V(z)}-v_0\right)^2\right). \qquad (11)$$

The Poisson equation for the system is written as:

$$V_1''(z) = -\frac{q}{\varepsilon_0}\left(\int_0^\infty f_z(v_z)dv_z + \int_0^{\sqrt{2\eta(V(z)-V_m)}} f_z(v_z)dv_z\right) \qquad (12)$$

for $0<z<X_m$, and

$$V_2''(z) = -\frac{q}{\varepsilon_0}\int_{\sqrt{2\eta(V(z)-V_m)}}^\infty f_z(v_z)dv_z \qquad (13)$$

for $X_m<z<d_r$.

Here, V_m is the magnitude of the potential minimum. In Eq. (12), the contribution of particle density comes from both forward particles and backward particles reflected back from the potential minimum at X_m. In Eq.(13), there are only forward particles.

Eqs. (12) and (13) can be numerically solved with appropriate boundary conditions. One example of the simulation results is shown in Fig. 3, where the input beam has mean energy of 5.070 keV and rms energy spread of 2.2 eV. The normalized current density λ is 0.062 and 1.2 respectively. Fig. 3(a) depicts the potential distribution for retarding voltage Vr= -5070 V. For small current (λ=0.062), The potential monotonically decreases from ground to V_r. For large space charge (λ=1.2), the potential distribution has a potential minimum, which is about 7 V below the retarding voltage. Fig. 3(b) shows the calculated spectrum for λ=0.062 and λ=1.2 respectively. At small current density, the device can reveal true beam spectrum, which has the rms energy spread of 2.2 eV. At high current density case, the spectrum is shifted towards the low energy side by 20 eV and becomes a delta function with zero energy width. In this case, the information of the rms energy spread and FWHM is totally lost. This is due to the abrupt formation of the potential minimum in the one-dimensional theory. In the real device, the potential at the beam edge will not be depressed as deeply as predicted by the one-dimensional theory. To illustrate this two-dimensional consideration without putting the effort to have a full 2D simulation, we build a simple model to have a 2D correction. At the center of the beam, we use the calculated value based on the 1D theory. At the edge of the beam, we set the value as $V=w*V_m+(1-w)*V_r$, which is the weighted average of the potential minimum, V_m and the retarding potential V_r.

In between, the potential increases quadratically from the center value to the edge value. This implies that we assume the particle density is uniform inside the beam. Fig. 3(c) depicts the result of this correction, which has a wider spectrum, and with a tail at the high-energy side. In this calculation, w is chosen as 0.685. This simple analysis shows the difference between the two-dimensional situation and the 1D theory. It indicates the necessity to have a full two-dimensional simulation. Another limitation of the theory is that this is a steady state solution. In reality, both magnitude and position of the potential minimum oscillate [8]. This will also make the energy spectrum wider than a delta function in the real situation.
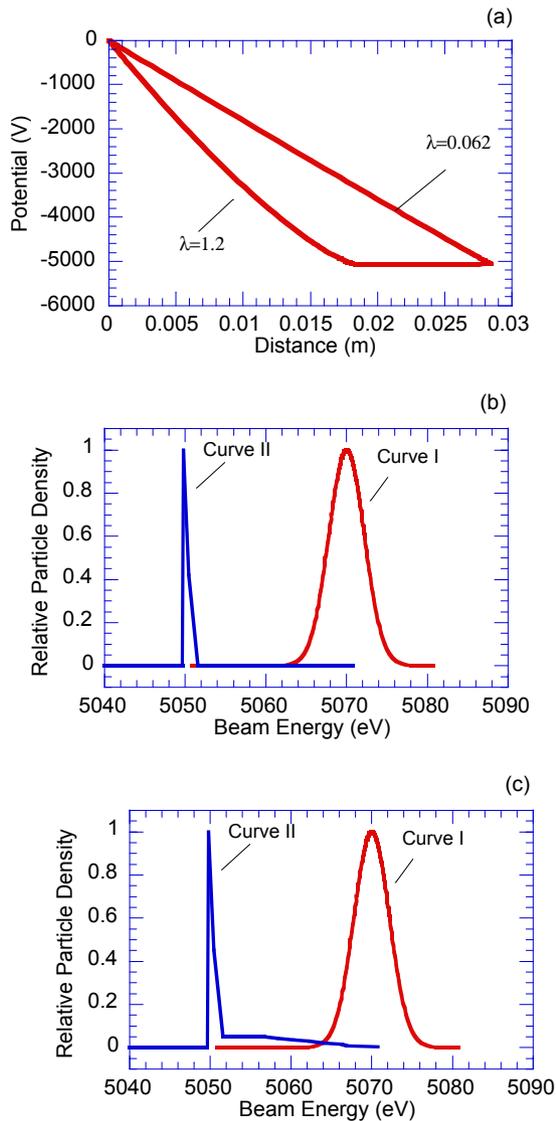
Fig. 3. (a) Potential distribution. (b) Energy spectrum. Curve I for λ=0.062, curve II for λ=1.2 (c) Energy spectrum with 2D correction. Curve I for λ=0.062, curve II for λ=1.2

CONCLUSION

The experimental and theoretical study shows that, if the current density inside the device is high enough, the space-charge effect could impact the performance of the energy analyzer. Specifically, the longitudinal space charge has three effects on the measurement. First, it will make the measured mean energy shifted toward the low-energy side. Second, it will cause a tail at the high-energy side. Third, it will affect the accuracy of FWHM and rms energy spread measurement. These effects are the artifacts of the device and we should avoid them in the experiment. According to the theory, if the normalized current density is below a critical value (λ=0.5), the longitudinal space-charge force does not affect the measurement any more. Therefore, we should keep the current density inside the device low for reducing the space-charge effect. The limitation of the theory lies in that this is a one-dimensional theory and we only solved the steady-state solution. A two-dimensional simulation with a PIC code is under way to study this problem in more detail.

ACKNOWLEDGEMENT

REFERENCES

[1] P.G. O'Shea, M. Reiser, R.A. Kishek, S. Bernal, H. Li, M. Pruessner, V. Yun, Y. Cui, W. Zhang, Y. Zou, T. Godlove, D. Kehne, P. Haldemann, and I. Haber, "*The University of Maryland Electron Ring"*, Nucl. Instr. and Meth. A **464**, 2001, p. 646-652.

[2] Y. Zou, Y. Cui, V. Yun, A. Valfells, R.A. Kishek, S. Bernal, I. Haber, M. Reiser, P.G. O'Shea, and J.G. Wang, "*Compact high-resolution retarding field energy analyzer for space-charge-dominated electron beams"*, Phys. Rev. ST Accel. Beams **5**(7), 2002, p. 011502.

[3] Y. Cui, Y. Zou, I. Haber, R. Kishek, P.G. O'Shea, M. Reiser, and A. Valfells, "*Experimental Study of Beam Energy Spread in the Space-Charge Dominated Beams"*, in *this proceeding*, 2003.

[4] T. Honzawa, T. Sekizawa, Y. Miyauchi, and T. Nagasawa, "*Effects of Space Charges in Gridded Energy Analyzer"*, Jpn. J. Appl. Phys. **32**(12A), 1993, p. 5748.

[5] G. Donoso and P. Martin, "*Space-charge effects in a velocity analyzer of variable geometry"*, Rev. Sci. Instrum. **61**(11), 1990, p. 3381.

[6] P. Martin and G. Donoso, "*A new Langmuir-Child equation including temperature effects"*, Phys. Fluids B **1**(1), 1988, p. 247.

[7] Y. Zou, H. Li, M. Reiser and P.G. O'Shea, "*Theoretical Study of Transverse Emittance Growth in a Gridded Electron Gun*", submitted to NIM.

[8] I. Haber, private communication.